


# Josephson Parametric Reflection Amplifier with Integrated Directionality

M. P. Westig\* and T. M. Klapwijk†

*Kavli Institute of NanoScience, Delft University of Technology, Lorentzweg 1,  
2628 CJ Delft, The Netherlands*

 (Received 28 June 2017; revised manuscript received 29 March 2018; published 11 June 2018)

A directional superconducting parametric amplifier in the GHz frequency range is designed and analyzed, suitable for low-power read-out of microwave kinetic inductance detectors employed in astrophysics and when combined with a nonreciprocal device at its input also for circuit quantum electrodynamics. It consists of a one-wavelength-long nondegenerate Josephson parametric reflection amplifier circuit. The device has two Josephson-junction oscillators, connected via a tailored impedance to an on-chip passive circuit which directs the in- to the output port. The amplifier provides a gain of 20 dB over a bandwidth of 220 MHz on the signal as well as on the idler portion of the amplified input and the total photon shot noise referred to the input corresponds to maximally approximately 1.3 photons per second per Hertz of bandwidth. We predict a factor of 4 increase in dynamic range compared to conventional Josephson parametric amplifiers.

DOI: [10.1103/PhysRevApplied.9.064010](https://doi.org/10.1103/PhysRevApplied.9.064010)

## I. INTRODUCTION

Nonlinearities in superconducting devices, such as the nonlinear Josephson inductance [1], are building blocks for parametric amplification. They can be employed in low-noise Kerr-type nonlinear oscillators, providing three- or four-wave mixing interactions [2,3] enabling degenerate (phase sensitive) or nondegenerate (phase preserving) operation [4]. In this article, we design and analyze such a parametric amplifier with integrated directionality, facilitating emerging low-power read-out schemes for microwave kinetic inductance microresonator detectors (MKID) [5,6] employed in astrophysics instruments. While our amplifier concept is directional although reciprocal, it is only one wavelength long, which suits and further integrates the MKID read-out back end. Recent findings suggest that the vacuum noise generated at the input of our parametric amplifier does not decrease the sensitivity of the MKID. State-of-the-art read-out schemes of this detector use read-out photon numbers of many hundreds of millions in order to overcome the cryogenic high electron-mobility amplifier noise and often no circulators are used between the detector and the read-out amplifier [5]. It is expected, however, that the MKID sensitivity can be further increased by reducing the read-out photon number, which can be achieved by parametric amplifiers [6] such as Josephson parametric amplifiers (JPA). Eventually this will help to uncover fundamental sources of two-level system noise in superconducting microresonators of which no

microscopic theory yet exists, important for detectors but also for quantum information processors. In order to be practicable in view of the complete detection instrument, maybe first in small arrays of about 100 MKID detectors, the amplifier bandwidth has to be several tens of a MHz large, the dynamic range should enable us to process first up to, on average, 100 read-out photons and the amplifier should be directional, compact in size, and easy to fabricate.

A second application of our amplifier could be in a circuit quantum electrodynamics (cQED) [7–14] measurement scheme. In this case, our amplifier would have to be supplemented by a nonreciprocal device at its input to filter out the vacuum noise that would otherwise increase the parasitic photon population of a quantum sensitive device connected to the input. Also, few other parasitic photons could arise at the input of the parametric amplifier due to a finite return loss of the amplifier. Research on novel nonreciprocal device technologies without lossy and possibly disturbing magnetic materials, is presently an active field and is expected to provide adequate solutions soon. Here, techniques are employed from cavity optomechanics [15–22] over emulation of circulators with parametric active devices [23] or with Wheatstone bridge-based superconducting LC resonators [24,25]. Also, innovative techniques in cQED [26–30] and different Josephson parametric converter circuits [31–33] as well as other directional Josephson circuits [34,35] have been realized. Together with the integrated directionality of our amplifier, it is very likely that the parasitic photon population of a quantum sensitive device connected to the nonreciprocal device-parametric amplifier combination is effectively reduced. The nonreciprocal device would have to filter

\*m.p.westig@tudelft.nl

†t.m.klapwijk@tudelft.nl

out only the vacuum noise and not direct additionally the amplified field to the measurement chain which is separately achieved by our amplifier concept.

## II. AMPLIFIER DESIGN AND PERFORMANCE

### A. General concept

Our amplifier is operated close to its bifurcation point when the dynamics are that of a Duffing oscillator, a small input signal change induces a large variation in the system dynamics leading to amplification [36–39].

Figure 1(a) shows the aluminum microstrip circuit of the JPA. Essential elements are a superconducting branch-line coupler (like we have realized experimentally in Refs. [40,41]) and an embedding circuit which is connected to two individual rf-shunted nonlinear Josephson-junction oscillators (JJO), operated at approximately 10 mK. The branch-line coupler combines the individual JJOs to a single JPA [42] and provides signal directivity while the matched input admittance  $Y_{in}^{''''}$  of the embedding circuit determines gain, noise, and bandwidth of the JPA via its engineered conductance and susceptance portions. The value of  $Y_{in}^{''''}$  is dominated by a capacitive shunt of the first  $\lambda/12$  section in the embedding circuit rather than by a higher-impedance inductive load, as realized in earlier work [43,44].

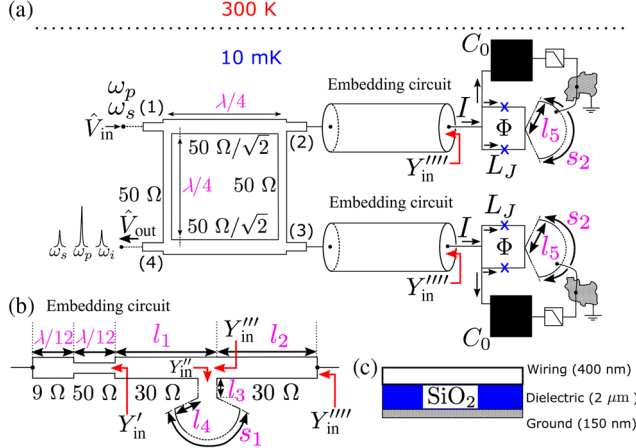


FIG. 1. *JPA with directionality.* (a) Top view on the 400-nm wiring of the aluminum microstrip circuit, consisting of three essential elements: branch-line coupler with ports (1)–(4), embedding circuit, and Josephson-junction oscillators with inductance  $L_J$  (crosses) and capacitance  $C_0$ . A signal  $\hat{V}_{in}$  having frequency  $\omega_s$  and injected in (1) along with a strong pump tone of frequency  $\omega_p$  is amplified and directed to (4). Additionally, amplified vacuum noise is emitted from input port (1) because of the reciprocity of the device. Also, few other parasitic photons could arise at the input due to a finite return loss of the amplifier. (b) Details of the embedding circuit of the best performance JPA[−0.36, +0.36], cf. Table I. (c) Cross-section of microstrip layers.

Each of the two JJOs should be characterized by the same plasma frequency  $\omega_0 = \{[2\pi I_c(\Phi)]/(\phi_0 C_0)\}^{-1/2}$ . Here,  $L_J(\Phi) = \phi_0/[2\pi I_c(\Phi)]$  is the Josephson inductance, being 0.12 nH in our case and  $C_0 = 4.0$  pF is the shunting capacitor. Furthermore,  $\phi_0 = h/(2e)$  is the flux quantum and  $I_c(\Phi) = 2i_c |\cos(\pi\Phi/\phi_0)|$  is the total critical current for each Josephson SQUID shown in Fig. 1(a), with  $i_c$  being the individual currents of the single junctions in the SQUID. An externally applied small magnetic flux bias  $\Phi$  induced in the SQUID loop tunes  $\omega_0/(2\pi) \sim 7.3$  GHz and the JJO admittance  $Y_0 = \sqrt{C_0/L_J(\Phi)}$ . The JJOs are pumped through their embedding circuit by a strong coherent tone of frequency  $\omega_p/(2\pi) \sim 6.0$  GHz which provides the energy for the amplification and by a much weaker quantum signal of frequency  $\omega_s$  which shall be amplified. In this work, we consider nondegenerate four-wave mixing as the amplifying mechanism for which  $2\omega_p = \omega_s + \omega_i$ ; two pump photons at  $\omega_p$  transfer their energy into signal and idler modes symmetric around  $\omega_p$ , cf. Fig 1(a). The Josephson SQUIDs are designed on top of a 2- $\mu\text{m}$ -thick  $\text{SiO}_2$  dielectric layer, cf. Fig. 1(c). Each of the SQUIDs is rf shunted through a virtual short around 6 GHz, realized by a broadband radial stub tuner [45] with dimensions  $\{s_2, l_5\}$  and characteristic input impedance of 50  $\Omega$ . A bonding wire connects the edge of the radial stub directly to an island on the ground plane, connecting the otherwise galvanically separated microstrip layers. On the other side of the SQUID, the same island connects to a planar low-pass filter (e.g., a standard microstrip Chebyshev rf-blocking filter [46]), being connected to the oscillator's shunting capacitor  $C_0$ . Therefore, a dc current can flow through the SQUID, providing the inductance  $L_J$ , and at the same time the bonding wires do not disturb the rf circuit.

### B. Equation of motion, gain, and noise

The equation of motion (EOM) for each of the two JJOs is described by independent Duffing equations obtained from the RCSJ model [47] and by Kirchhoff's law applied to the equivalent circuit of the JJO and its embedding circuit, shown in Figs. 1(a) and 1(b):

$$\ddot{\delta}(t) + \kappa\dot{\delta}(t) + \omega_0^2 \left[ \delta(t) - \frac{\delta(t)^3}{6} \right] - \omega_0^2 \frac{I_p(t)}{I_c(\Phi)} = \frac{4\pi\hat{I}_{in}(t)}{\phi_0 C_0}. \quad (1)$$

This equivalent circuit describes the pumping of the particular JJO from a (parallel) current source with admittance  $Y_{in}^{''''}$ . Furthermore,  $\delta(t) = \delta_p(t) + \hat{\delta}_s(t)$  is the intra-oscillator field and consists of a classical term  $\delta_p(t)$  due to the coherent large amplitude pump tone,  $I_p(t) = \bar{I}_p \cos(\omega_p t)$ , and a quantum term  $\hat{\delta}_s(t)$  induced by the weak signal  $\hat{I}_{in}(t)$ . The dissipation is quantified by a rate

$\text{Re}[\kappa] = \text{Re}[Y_{\text{in}}^{\text{eff}}]/C_0$ , obtaining the convenient value  $\text{Re}[\kappa]/(2\pi) \sim 1.33$  GHz. Equation (1) only holds for a strong nonlinearity of the JJO compared to the linear inductance  $L_{\text{env}}$  contributed by the embedding circuit. This is quantified by the participation ratio  $p = L_{\parallel}/L_J$  [39] and  $L_{\parallel}^{-1} = L_{\text{env}}^{-1} + L_J^{-1}$ , where  $L_{\parallel}$  is the total parallel inductance. We find that  $L_{\text{env}}$  is larger by about a factor of 22 compared to  $L_J$  so that the nonlinearity of the JJO is strong enough to assume the ideal case provided by Eq. (1), where the nonlinear term reads  $p\delta(t)^3/6 \approx \delta(t)^3/6$ . For  $\hat{I}_{\text{in}} = 0$ , one obtains the steady-state solution of Eq. (1) which determines the classical pump intraoscillator field  $\delta_p(t)$  with maximum amplitude  $\delta_{p,\text{max}}$ .

The case  $\hat{I}_{\text{in}} \neq 0$  obtains the quantum intraoscillator field by subtracting the steady-state solution from Eq. (1). We proceed by making a Fourier transformation and subsequent transition into the rotating frame [48] of the pumping field at frequency  $\omega_p$ , obtaining

$$\left[ i(\tilde{\Omega}_p - \tilde{\omega}_s) + \frac{\kappa[\tilde{\omega}_s]}{2} \right] \hat{a}_s[\tilde{\omega}_s] - \frac{i\omega_0\delta_{p,\text{max}}^2}{16} \hat{a}_i^\dagger[-\tilde{\omega}_s] = \hat{a}_{\text{in}}[\tilde{\omega}_s]. \quad (2)$$

We denote with  $\tilde{\Omega}_p = \omega_0 - \omega_p - \omega_0\delta_{p,\text{max}}^2/8$  the effective pump-frequency detuning and with  $\tilde{\omega}_s = \omega_p - \omega_s$  the signal-frequency detuning. The intraoscillator field operators  $\hat{a}_{s,i}$  describing the signal and idler modes are related up to a phase factor to  $\hat{\delta}_s$ . They obey the standard Heisenberg EOM of the nondegenerate JPA [49,50] through the four-wave-mixing Hamiltonian  $\hat{H} = \hbar\tilde{\Omega}_p(\hat{a}_s^\dagger\hat{a}_s + \hat{a}_i^\dagger\hat{a}_i) + i\hbar(g/2)(\hat{a}_s^\dagger\hat{a}_i^\dagger - \hat{a}_s\hat{a}_i)$ , where  $g = 2\Lambda\bar{n}$  is a Kerr-like nonlinearity [8,50] with  $\Lambda\bar{n} \sim \omega_0\delta_{p,\text{max}}^2/16$  being the product of oscillator nonlinearity and the large average number of quanta  $\bar{n} \gg 1$  in the oscillator. The solution of the Heisenberg EOM gives the oscillator susceptibility, linking the intraoscillator field to the input field. The inverse susceptibility matrix  $\chi^{-1}$  is the coefficient matrix of Eq. (2) and its adjoint equation;  $\chi[\tilde{\omega}_s]^{-1} \cdot \hat{\mathbf{a}}[\tilde{\omega}_s] = \hat{\mathbf{a}}_{\text{in}}[\tilde{\omega}_s]$ , where  $\hat{\mathbf{a}}_{\text{in}} = (\hat{a}_{\text{in}}[\tilde{\omega}_s], \hat{a}_{\text{in}}^\dagger[-\tilde{\omega}_s])^T$ , and  $\hat{\mathbf{a}} = (\hat{a}_s[\tilde{\omega}_s], \hat{a}_i^\dagger[-\tilde{\omega}_s])^T$  [8,44]. By inverting  $\chi^{-1}$  and evaluating the element  $\chi_{11}$ , we determine the photon number gain  $G_s[\tilde{\omega}_s] = \mathcal{C}_1 |1 - \text{Re}[\kappa[\tilde{\omega}_s]]\chi_{11}[\tilde{\omega}_s]|^2$  which can be understood as a reflection coefficient at the JJO larger than one and  $\mathcal{C}_1$  is a circuit-dependent correction factor. A similar equation holds for the idler field. Knowing the gain, we can estimate the noise added by the nondegenerate JPA by using Ref. [50]. We modify their result to account for the complete noise referred to the input of the amplifier, consisting of a minimum of half a photon of shot noise per second and per Hz of bandwidth amplified from the signal and also from the idler field; in total  $T_N[\tilde{\omega}_s] = \mathcal{C}_2^{-1} \{ \hbar\omega_p/k_B - (2\hbar\tilde{\omega}_s/k_B) [\{1/4 + (G[0]/3) \times \omega/(1+\omega^2)\}^{1/2} - (G[0]/3)^{1/2}\omega/(1+\omega^2)] \}$ . Here,  $\mathcal{C}_2$  is

another circuit-dependent correction factor and  $\omega = \tilde{\omega}_s|\chi_{11}[0]|$ . For  $\tilde{\omega}_s = 0$  this is the fundamental result of the Haus-Caves theorem [4,51] and for  $\tilde{\omega}_s \neq 0$  we obtain an approximate relation of the noise in our amplifier for small detuning.

### C. Embedding circuit

We now describe how the two independent JJOs function as one single JPA via their surrounding circuit, cf. Fig. 1(a). The strong coherent pump tone is applied together with the weak quantum signal to the same input port (1) of a superconducting branch-line coupler. Our amplifier concept contributes a passive and ultra-low-loss signal routing functionality to the circuit toolbox that can in cQED applications be combined with existing nonreciprocal circuits to filter out parasitic photons that are generated at the input port (1) of our amplifier. The voltage amplitudes which propagate to ports (2), (3), and (4) are described by a scattering relation,  $[\mathbf{S}][\mathbf{V}^\rightarrow] = [\mathbf{V}^\leftarrow]$ , where  $[\mathbf{V}^\rightarrow, \leftarrow]$  are the ingoing ( $\rightarrow$ ) and outgoing ( $\leftarrow$ ) four-component voltage waves applied to ports (1)–(4) and

$$[\mathbf{S}] = (1/\sqrt{2}) \begin{pmatrix} 0 & 1 & i & 0 \\ 1 & 0 & 0 & i \\ i & 0 & 0 & 1 \\ 0 & i & 1 & 0 \end{pmatrix}$$

is unitary for a lossless ideal branch-line coupler. An input voltage  $V^\rightarrow = V_p[\omega_p]\exp(-i\theta_p) + \hat{V}_{\text{in}}[\omega_s]\exp(-i\theta_s)$  applied only to port (1), is divided equally between ports (2) and (3) together with a *relative* phase shift of  $\pi/2$ . Port (4) receives no signal in this case. The divided signals leaving ports (2) and (3) couple via the embedding circuits of dimensions  $\{l_i, s_i\}$  to the JJOs in which they are amplified and reflected. Ideally, the reflected signals still carry this *relative* phase shift of  $\pi/2$  and are back coupled to ports (2) and (3). An evaluation of the output voltages via the  $[\mathbf{S}]$  matrix shows that now the divided signals combine again constructively at port (4), whereas port (1) receives no signal. We visualize this effect in Fig. 2 and show that the routing of the signals in our circuit is entirely passive and not susceptible to loss within the amplifier bandwidth. For a nondegenerate JPA which preserves the input phase(s) at the output [4], we assume without loss of generality  $\theta_p = \theta_s = \pi/2$  at port (1). The density plots for the electric field between the ground plane and the wiring circuit [cf. Fig. 1(c)],  $|\mathbf{E}(\mathbf{r})|$ , using this choice of phases shows the directional operation on the branch-line coupler. The calculated scattering parameter magnitudes for our circuit are shown in the same figure. They are related to powers ( $\propto V^2$ ) and quantify the signal distribution, yielding an almost perfect realization of the ideal  $[\mathbf{S}]$  matrix over the envisioned operation bandwidth of the JPA.

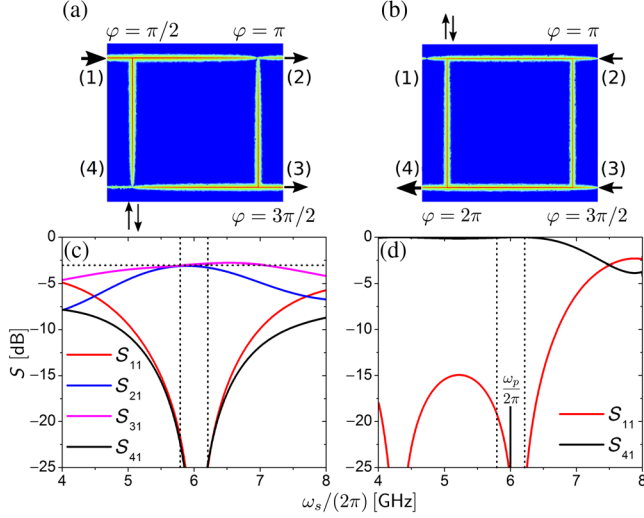


FIG. 2. *Directionality.* (a) and (b) show a snapshot of  $|\mathbf{E}(\mathbf{r})|$  on the branch-line coupler at the design frequency 6 GHz. (c) and (d) quantify the corresponding scattering parameters, determining a slight asymmetry in the coupler performance. Note that in (d) the scattering parameters are fully reciprocal, in particular  $S_{41} = S_{14}$ . Hence, vacuum noise is generated at input port (1). In applications for cQED this noise has to be filtered out by an additional nonreciprocal device connected to input port (1). (a) Excitation of port (1) and phase-delayed distribution to ports (2) and (3) connecting to the amplifier circuits (not shown); port 4 receives no signal and this is indicated by the up-down arrows illustrating an out-of-phase condition. (b) Returning phase-delayed signals from the amplifier circuits, combining this time in-phase at the output port (4) and not at port (1), quantified by the value  $S_{11}$ . In (b) the gain is set to  $G = 1$  for illustrative purposes. Vertical dashed lines are taken from Fig. 4(b) indicative of the amplifier  $-3$  dB bandwidth and the horizontal dashed line is the  $-3$  dB level of the branch-line coupler.

We design the embedding circuit by visualizing the voltage reflection coefficient and, hence, the normalized complex transmission-line input admittance  $Y_{in}/Y_c = [Y_L + iY_c \tanh(\gamma l)]/[Y_c + iY_L \tanh(\gamma l)]$  in the polar plane of the Smith chart [46,52], cf. Figs. 1(a) and 3(a). Here,  $Y_c$  is the characteristic admittance of the particular microstrip segment,  $Y_L$  is the termination admittance,  $\gamma$  is the complex propagation constant [48,53], and  $l$  is the length. Finally, the complex valued admittance is plotted in the Smith chart. A point represents the intersection between the corresponding conductance circle, where the normalized conductance is indicated on the horizontal axis and the susceptance circle, where the normalized susceptance is indicated around the Smith chart. For a given admittance, a change in  $l$  will rotate the trace in the Smith chart by  $2\gamma l$  and connecting admittances of different values will lead to jumps in the overall admittance [compare with the traces in Fig. 3(a)], transforming the admittance and changing the shape of the conductance and the slope of the susceptance of  $Y_{in}^{(m)}$  as shown in Fig. 3(b). The correction factors for gain and noise are given by the scattering parameters and the

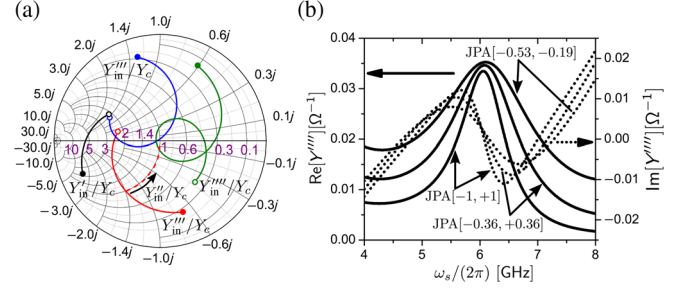


FIG. 3. *Embedding circuit design.* (a) The Smith chart shows the design-relevant input admittances in the polar plane, normalized to the characteristic admittance of the particular circuit part, extracted from Table I for the case of JPA  $[-0.36, +0.36]$ . The shunting capacitance which is encoded in the trace  $Y_{in}^{(m)}$  determines the shape of the desired admittance  $Y_{in}^{(m)}$ , controlling the amplifier performance. The red and blue traces are the admittances before and after shunting with the stub with admittance  $Y_{in}^{(m)}$ , pulling the red trace into the vicinity of the desired green trace. The open and closed circles indicate the start (4 GHz) and stop (8 GHz) frequency. (b) Separate real (conductance) and imaginary (susceptance) components of  $Y_{in}^{(m)}[\omega_s/(2\pi)]$  for a single embedding circuit used in the three designs.

coupling to the JJOs,  $C_1 = |S_{41}[\tilde{\omega}_s]|$  shown in Fig. 2(d) and  $C_2 = (|S_{21}[\tilde{\omega}_s]| + |S_{31}[\tilde{\omega}_s]|) \times \mathcal{T}$  where the scattering parameters are the ones shown in Fig. 2(c) and  $\mathcal{T}$  is the signal coupling to the JJOs, being a factor between 1 and 0.95, cf. Ref. [48].

The directional signal routing in our device relies fundamentally on the imposed relative phase difference of  $\pi/2$  between the two JJOs and we have to estimate the influence of slightly detuned JJOs. We find that a relative plasma frequency detuning of 200 MHz will cause an

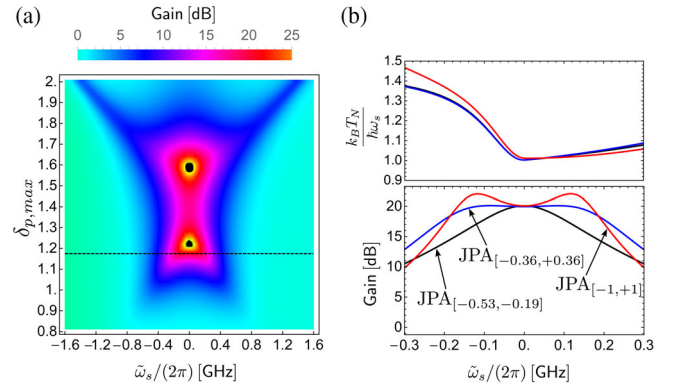


FIG. 4. *Amplifier performance.* (a) Power gain as a function of signal-frequency detuning  $\tilde{\omega}_s$  and pumping amplitude  $\delta_{p,max}$  for JPA  $[-0.36, +0.36]$ . The black dashed line indicates the optimal (lowest power) pumping amplitude to achieve a flat gain profile of about 20 dB. Black regions distinguish high-gain regimes  $\gg 25$  dB but with significantly decreased bandwidth. (b) Approximate shape of the noise temperature referred to the input and optimal power gain as a function of signal-frequency detuning for the three designs.

TABLE I. Three JPA designs resulting in different residual frequency-dependent imaginary parts in  $-i\tilde{\omega}_s + \kappa[\tilde{\omega}_s]/2 \propto Y_{\text{in}}^{\text{''''}}[\tilde{\omega}_s]$  of Eq. (2). We quantify the residue by indicating the minimum and maximum slope of the imaginary part as index, e.g., JPA $[-0.36, +0.36]$ . A weakly frequency-dependent imaginary part with a slope symmetric around zero yields a maximal bandwidth determined by  $\text{Re}(Y_{\text{in}}^{\text{''''}}[\tilde{\omega}_s])$ . The numbers specify the dimensions of the circuit parts in micrometers from which the characteristic impedance in ohms is given in curly brackets.

Elements	JPA $[-1, +1]$	JPA $[-0.36, +0.36]$	JPA $[-0.53, -0.19]$
$\lambda/4$ [(1)-(2)] <sup>a</sup>	7098 $\{50/\sqrt{2}\}$	7098 $\{50/\sqrt{2}\}$	7098 $\{50/\sqrt{2}\}$
$\lambda/4$ [(1)-(4)] <sup>b</sup>	7306 $\{50\}$	7306 $\{50\}$	7306 $\{50\}$
$\lambda/12$ [first]	1177 $\{5\}$	1522 $\{9\}$	1941 $\{16\}$
$\lambda/12$ [second]	1332 $\{50\}$	1722 $\{50\}$	2077 $\{50\}$
$l_1$	1587 $\{30\}$	2137 $\{30\}$	2650 $\{30\}$
$l_2$	8815 $\{30\}$	9515 $\{30\}$	10262 $\{30\}$
$l_3$	262 $\{30\}$	182 $\{30\}$	182 $\{30\}$
$l_4$	290	224	155
$s_1$	658	553	422
$l_5$	2598	2598	2598
$s_2$	4848	4848	4848

<sup>a</sup>The connection of ports (3) and (4) has the same length.

<sup>b</sup>The connection of ports (2) and (3) has the same length.

additional phase difference of approximately  $\pi/18$  in the outgoing amplified signals. While this will only slightly change the coupler directivity  $S_{41}$  in Fig. 2(d), the return loss  $S_{11}$  of the device port (1) indicated in the same figure will degrade to  $-12$  dB from its original value of  $< -25$  dB [48]. In the aforementioned situation, the two JJOs differ also in their gain by about 0.8 dB, which has a negligible influence.

### III. RESULTS

Figure 4 and Table I summarize our results for gain, noise, and the designs of the JPA. While we obtain the best performance for JPA $[-0.36, +0.36]$ , the other two designs show the influence of the real and imaginary part of  $Y_{\text{in}}^{\text{''''}}$  on the amplifier performance. For design JPA $[-0.36, +0.36]$ , the term  $-\tilde{\omega}_s + \text{Im}[\kappa[\tilde{\omega}_s]]$  in Eq. (2) assumes the smallest frequency dependence with a slope symmetric around zero, maximizing the amplification bandwidth. For the other two designs the same term contains a much stronger frequency dependence and the slope is not symmetric around zero, resulting in a decreased performance, and therefore, bandwidth of the amplifier. The dynamic range for a single Josephson-junction oscillator operated close to the bifurcation point scales with  $P_{\text{dyn}} \propto I_c^2/Q$  [39], where  $Q \approx \omega_0 \text{Re}[Z_{\text{in}}^{\text{''''}}]C_0$ . The two JJOs in our circuit effectively double the critical current, which increases the dynamic range by a factor of 4.

It can be further increased by increasing the current density of the Josephson junctions, which is rather limited for Al/AIOx/Al junctions. Higher values of up to  $J_c = 78$  kA/cm<sup>2</sup> are reachable with AlN barriers in Nb-based circuits [54], which would increase the dynamic range by up to 3 orders of magnitude compared to existing JPAs and would enable the read-out of large arrays of detectors

containing some thousands of pixels [5] or multiple qubits [11]. In this amplifier technology, however, the SQUID cannot be fabricated anymore using the well-established angle-evaporation technique, and one has to rely on trilayer Josephson junctions [40,41].

### IV. DISCUSSION

We have designed and analyzed a broadband and compact JPA with integrated directionality which adds only about one single photon of total noise at the input. While our proposed device is fully reciprocal, nonreciprocity can be achieved by combining our device with existing nonreciprocal devices at the input of our amplifier. Employing existing high-current density Josephson junctions would increase the dynamic range significantly compared to existing JPAs. Our embedding circuit is general enough to tune the gain of signal and idler modes independently, providing interesting opportunities to tailor nonclassical microwave light [55,56].

In closing, we address two specific examples, where our proposed amplifier adds functionality.

In cQED, an increasing number of experiments reads out a cavity state by using a one-port JPA together with a nonreciprocal device, which directs the amplified field to the postprocessing electronics and protects the cavity from noise. Commercially available nonreciprocal magnetic circulators are mainly characterized by their isolation, which quantifies to what extent the circulator can block radiation emitted towards the quantum sensitive cavity. A typical isolation value for these commercial circulators amounts to  $-20$  dB. This is also true for the nonmagnetic circulator reported in Ref. [25]. As a consequence, the amplified vacuum noise of such a one-port JPA, emitted

towards the nonreciprocal device, results in one parasitic photon per second and per Hz of bandwidth, transmitted towards the cavity. A desired cavity field, amplified by the JPA, will further enhance the number of these parasitic photons. Improvement over a broad bandwidth is difficult to achieve.

Our amplifier concept provides an attractive solution since it emits only amplified vacuum noise from input port (1) and emits separately the amplified field and vacuum noise from output port (4). Therefore, a nonreciprocal device with a given isolation connected to input port (1), reduces also the parasitic photons transmitted through the nonreciprocal device towards the cavity.

In another example, in astronomical instrumentation [57,58] microresonator arrays of 20 000 pixels have been realized recently. The dissipation and the noise of the read-out amplifiers is becoming a very important limiting factor. In addition, in order to reduce standing waves in the read-out signal it would be beneficial to integrate an amplifier on the same chip with the MKID array. The fabrication of our amplifier is compatible with the currently used MKID technology. Our amplifier concept makes it possible to connect the read-out line of the MKID array directly to input port (1). The combination of low noise, broadband, and integrability make our proposed amplifier very suitable for use with MKID arrays.

### ACKNOWLEDGMENTS

We acknowledge funding through the European Research Council Advanced Grant No. 339306 (METIQUM). We have had fruitful discussions with Karl Jacobs and Patrick Pütz of KOSMA, I. Physikalisches Institut, Universität zu Köln, Germany, related to the microfabrication of the circuit and the various Josephson-junction technologies. Furthermore, we appreciate helpful comments from Udson Mendes, Université de Sherbrooke, Canada, on the general content. We would like to thank the referees for critical and essential comments on the input noise created by our parametric amplifier and for other general comments which helped to improve the manuscript.

---

[1] B. D. Josephson, Coupled superconductors, *Rev. Mod. Phys.* **36**, 216 (1964).  
 [2] B. Yurke, P. G. Kaminsky, R. E. Miller, E. A. Whittaker, A. D. Smith, A. H. Silver, and R. W. Simon, Observation of 4.2-K Equilibrium-Noise Squeezing via a Josephson-Parametric Amplifier, *Phys. Rev. Lett.* **60**, 764 (1988).  
 [3] B. Yurke, L. R. Corruccini, P. G. Kaminsky, L. W. Rupp, A. D. Smith, A. H. Silver, R. W. Simon, and E. A. Whittaker, Observation of parametric amplification and deamplification in a Josephson parametric amplifier, *Phys. Rev. A* **39**, 2519 (1989).

[4] C. M. Caves, Quantum limits on noise in linear amplifiers, *Phys. Rev. D* **26**, 1817 (1982).  
 [5] P. K. Day, H. G. LeDuc, B. A. Mazin, A. Vayonakis, and J. Zmuidzinas, A broadband superconducting detector suitable for use in large arrays, *Nature (London)* **425**, 817 (2003).  
 [6] J. Zmuidzinas, Superconducting microresonators: Physics and applications, *Annu. Rev. Condens. Matter Phys.* **3**, 169 (2012).  
 [7] M. H. Devoret and R. J. Schoelkopf, Superconducting circuits for quantum information: An outlook, *Science* **339**, 1169 (2013).  
 [8] A. A. Clerk, M. H. Devoret, S. M. Girvin, F. Marquardt, and R. J. Schoelkopf, Introduction to quantum noise, measurement and amplification, *Rev. Mod. Phys.* **82**, 1155 (2010).  
 [9] A. Bienfait, J. J. Pla, Y. Kubo, M. Stern, X. Zhou, C. C. Lo, C. D. Weis, T. Schenkel, M. L. W. Thewalt, D. Vion, D. Esteve, B. Julsgaard, K. Mølmer, J. J. L. Morton, and P. Bertet, Reaching the quantum limit of sensitivity in electron spin resonance, *Nat. Nanotechnol.* **11**, 253 (2016).  
 [10] A. Bienfait, J. J. Pla, Y. Kubo, X. Zhou, M. Stern, C. C. Lo, C. D. Weis, T. Schenkel, D. Vion, D. Esteve, J. J. L. Morton, and P. Bertet, Controlling spin relaxation with a cavity, *Nature (London)* **531**, 74 (2016).  
 [11] R. Barends, J. Kelly, A. Megrant, A. Veitia, D. Sank, E. Jeffrey, T. C. White, J. Mutus, A. G. Fowler, B. Campbell, Y. Chen, Z. Chen, B. Chiaro, A. Dunsworth, C. Neill, P. O'Malley, P. Roushan, A. Vainsencher, J. Wenner, A. N. Korotkov, A. N. Cleland, and John M. Martinis, Superconducting quantum circuits at the surface code threshold for fault tolerance, *Nature (London)* **508**, 500 (2014).  
 [12] M. Hofheinz, H. Wang, M. Ansmann, R. C. Bialczak, E. Lucero, M. Neeley, A. D. O'Connell, D. Sank, J. Wenner, J. M. Martinis, and A. N. Cleland, Synthesizing arbitrary quantum states in a superconducting resonator, *Nature (London)* **459**, 546 (2009).  
 [13] M. Hofheinz, E. M. Weig, M. Ansmann, R. C. Bialczak, E. Lucero, M. Neeley, A. D. O'Connell, H. Wang, J. M. Martinis, and A. N. Cleland, Generation of Fock states in a superconducting quantum circuit, *Nature (London)* **454**, 310 (2008).  
 [14] F. Mallet, F. R. Ong, A. Palacios-Laloy, F. Nguyen, P. Bertet, D. Vion, and D. Esteve, Single-shot qubit readout in circuit quantum electrodynamics, *Nat. Phys.* **5**, 791 (2009).  
 [15] S. Barzanjeh, M. Wulf, M. Peruzzo, M. Kalaei, P. B. Dieterle, O. Painter, and J. M. Fink, Mechanical on-chip microwave circulator, *Nat. Commun.* **8**, 953 (2017).  
 [16] N. R. Bernier, L. D. Tóth, A. Koottandavida, M. Ioannou, D. Malz, A. Nunnenkamp, A. K. Feofanov, and T. J. Kippenberg, Nonreciprocal reconfigurable microwave optomechanical circuit, *Nat. Commun.* **8**, 604 (2017).  
 [17] G. A. Peterson, F. Lecocq, K. Cicak, R. W. Simmonds, J. Aumentado, and J. D. Teufel, Demonstration of Efficient Nonreciprocity in a Microwave Optomechanical Circuit, *Phys. Rev. X* **7**, 031001 (2017).  
 [18] K. Fang, J. Luo, A. Metelmann, M. H. Matheny, F. Marquardt, A. A. Clerk, and O. Painter, Generalized non-reciprocity in an optomechanical circuit via synthetic magnetism and reservoir engineering, *Nat. Phys.* **13**, 465 (2017).

- [19] F. Ruesink, M. Miri, A. Alú, and E. Verhagen, Non-reciprocity and magnetic-free isolation based on optomechanical interactions, *Nat. Commun.* **7**, 13662 (2016).
- [20] Z. Shen, Y.-L. Zhang, Y. Chen, C.-L. Zou, Y.-F. Xiao, X.-B. Zou, F.-W. Sun, G.-C. Guo, and C.-H. Dong, Experimental realization of optomechanically induced non-reciprocity, *Nat. Photonics* **10**, 657 (2016).
- [21] X.-W. Xu, Y. Li, A.-X. Chen, and Y.-X. Liu, Nonreciprocal conversion between microwave and optical photons in electro-optomechanical systems, *Phys. Rev. A* **93**, 023827 (2016).
- [22] M. Hafezi and P. Rabl, Optomechanically induced non-reciprocity in microring resonators, *Opt. Express* **20**, 7672 (2012).
- [23] A. Kamal, J. Clarke, and M. H. Devoret, Noiseless non-reciprocity in a parametric active device, *Nat. Phys.* **7**, 311 (2011).
- [24] J. Kerckhoff, K. Lalumière, B. J. Chapman, A. Blais, and K. W. Lehnert, On-Chip Superconducting Microwave Circulator from Synthetic Rotation, *Phys. Rev. Applied* **4**, 034002 (2015).
- [25] Benjamin J. Chapman, Eric I. Rosenthal, Joseph Kerckhoff, Bradley A. Moores, Leila R. Vale, J. A. B. Mates, Gene C. Hilton, Kevin Lalumière, Alexandre Blais, and K. W. Lehnert, Widely Tunable On-Chip Microwave Circulator for Superconducting Quantum Circuits, *Phys. Rev. X* **7**, 041043 (2017).
- [26] J. Koch, A. A. Houck, K. Le Hur, and S. M. Girvin, Time-reversal-symmetry breaking in circuit-QED-based photon lattices, *Phys. Rev. A* **82**, 043811 (2010).
- [27] A. Metelmann and A. A. Clerk, Nonreciprocal Photon Transmission and Amplification via Reservoir Engineering, *Phys. Rev. X* **5**, 021025 (2015).
- [28] L. Ranzani and J. Aumentado, Graph-based analysis of nonreciprocity in coupled-mode systems, *New J. Phys.* **17**, 023024 (2015).
- [29] A. Kamal, A. Roy, J. Clarke, and M. H. Devoret, Asymmetric Frequency Conversion in Nonlinear Systems Driven by a Biharmonic Pump, *Phys. Rev. Lett.* **113**, 247003 (2014).
- [30] N. A. Estep, D. L. Sounas, J. Soric, and A. Alú, Magnetic-free non-reciprocity and isolation based on parametrically modulated coupled-resonator loops, *Nat. Phys.* **10**, 923 (2014).
- [31] K. M. Sliwa, M. Hatridge, A. Narla, S. Shankar, L. Frunzio, R. J. Schoelkopf, and M. H. Devoret, Reconfigurable Josephson Circulator/Directional Amplifier, *Phys. Rev. X* **5**, 041020 (2015).
- [32] B. Abdo, K. Sliwa, S. Shankar, M. Hatridge, L. Frunzio, R. Schoelkopf, and M. Devoret, Josephson Directional Amplifier for Quantum Measurement of Superconducting Circuits, *Phys. Rev. Lett.* **112**, 167701 (2014).
- [33] B. Abdo, K. Sliwa, L. Frunzio, and M. Devoret, Directional Amplification with a Josephson Circuit, *Phys. Rev. X* **3**, 031001 (2013).
- [34] F. Lecocq, L. Ranzani, G. A. Peterson, K. Cicak, R. W. Simmonds, J. D. Teufel, and J. Aumentado, Nonreciprocal Microwave Signal Processing with a Field-Programmable Josephson Amplifier, *Phys. Rev. Applied* **7**, 024028 (2017).
- [35] C. Macklin, K. O'Brien, D. Hover, M. E. Schwartz, V. Bolkhovskoy, X. Zhang, W. D. Oliver, and I. Siddiqi, A near-quantum-limited Josephson traveling-wave parametric amplifier, *Science* **350**, 307 (2015).
- [36] R. Vijay, M. H. Devoret, and I. Siddiqi, Invited review article: The Josephson bifurcation amplifier, *Rev. Sci. Instrum.* **80**, 111101 (2009).
- [37] I. Siddiqi, R. Vijay, F. Pierre, C. M. Wilson, M. Metcalfe, C. Rigetti, L. Frunzio, and M. H. Devoret, RF-Driven Josephson Bifurcation Amplifier for Quantum Measurement, *Phys. Rev. Lett.* **93**, 207002 (2004).
- [38] I. Siddiqi, R. Vijay, F. Pierre, C. M. Wilson, L. Frunzio, M. Metcalfe, C. Rigetti, R. J. Schoelkopf, M. H. Devoret, D. Vion, and D. Esteve, Direct Observation of Dynamical Bifurcation between Two Driven Oscillation States of a Josephson Junction, *Phys. Rev. Lett.* **94**, 027005 (2005).
- [39] V. E. Manucharyan, E. Boaknin, M. Metcalfe, R. Vijay, I. Siddiqi, and M. Devoret, Microwave bifurcation of a Josephson junction: Embedding-circuit requirements, *Phys. Rev. B* **76**, 014524 (2007).
- [40] M. P. Westig, K. Jacobs, J. Stutzki, M. Schultz, M. Justen, and C. E. Honingh, Balanced superconductor-insulator-superconductor mixer on a 9  $\mu\text{m}$  silicon membrane, *Supercond. Sci. Technol.* **24**, 085012 (2011).
- [41] M. P. Westig, M. Justen, K. Jacobs, J. Stutzki, M. Schultz, F. Schomacker, and C. E. Honingh, A 490 GHz planar circuit balanced Nb-Al<sub>2</sub>O<sub>3</sub>-Nb quasiparticle mixer for radio astronomy: Application to quantitative local oscillator noise determination, *J. Appl. Phys.* **112**, 093919 (2012).
- [42] We study the functionality of the circuit by simulations in CST [59] and find consistence with an analytical model describing our microstrip geometry up to an uncertainty of 3% [48,53], assuming a normal-state resistance of  $\rho_n = 0.1 \mu\Omega\text{cm}$  and a superconducting gap of  $\Delta = 0.18 \text{ meV}$ .
- [43] J. Y. Mutus, T. C. White, R. Barends, Yu Chen, Z. Chen, B. Chiaro, A. Dunsworth, E. Jeffrey, J. Kelly, A. Megrant, C. Neill, P. J. J. O'Malley, P. Roushan, D. Sank, A. Vainsencher, J. Wenner, K. M. Sundqvist, A. N. Cleland, and J. M. Martinis, Strong environmental coupling in a Josephson parametric amplifier, *Appl. Phys. Lett.* **104**, 263513 (2014).
- [44] T. Roy, S. Kundu, M. Chand, A. M. Vadiraj, A. Ranadive, N. Nehra, M. P. Patankar, J. Aumentado, A. A. Clerk, and R. Vijay, Broadband parametric amplification with impedance engineering: Beyond the gain-bandwidth product, *Appl. Phys. Lett.* **107**, 262601 (2015).
- [45] R. Sorrentino and L. Roselli, A new simple and accurate formula for microstrip radial stub, *IEEE Microwave Guided Wave Lett.* **2**, 480 (1992).
- [46] R. E. Collin, *Foundations for Microwave Engineering* (Wiley-IEEE Press, Hoboken, New Jersey, 1992).
- [47] M. Tinkham, *Introduction to Superconductivity*, 2nd ed. (Dover Publications, Inc., Mineola, New York, 2004).
- [48] See Supplemental Material at <http://link.aps.org/supplemental/10.1103/PhysRevApplied.9.064010> for additional details.
- [49] C. W. Gardiner and M. J. Collett, Input and output in damped quantum systems: Quantum stochastic differential equations and the master equation, *Phys. Rev. A* **31**, 3761 (1985).

- [50] C. Laflamme and A. A. Clerk, Quantum-limited amplification with a nonlinear cavity detector, *Phys. Rev. A* **83**, 033803 (2011).
- [51] H. A. Haus and J. A. Mullen, Quantum noise in linear amplifiers, *Phys. Rev.* **128**, 2407 (1962).
- [52] P. H. Smith, Transmission line calculator, *Electronics* **12**, 29 (1939).
- [53] R. L. Kautz, Picosecond pulses on superconducting striplines, *J. Appl. Phys.* **49**, 308 (1978).
- [54] T. Zijlstra, C. F. J. Lodewijk, N. Vercruyssen, F. D. Tichelaar, D. N. Loudkov, and T. M. Klapwijk, Epitaxial aluminum nitride tunnel barriers grown by nitridation with a plasma source, *Appl. Phys. Lett.* **91**, 233102 (2007).
- [55] A. D. Armour, B. Kubala, and J. Ankerhold, Josephson photonics with a two-mode superconducting circuit, *Phys. Rev. B* **91**, 184508 (2015).
- [56] M. Westig, B. Kubala, O. Parlavecchio, Y. Mukharsky, C. Altimiras, P. Joyez, D. Vion, P. Roche, D. Esteve, M. Hofheinz, M. Trif, P. Simon, J. Ankerhold, and F. Portier, Emission of Non-Classical Radiation by Inelastic Cooper Pair Tunneling, *Phys. Rev. Lett.* **119**, 137001 (2017).
- [57] J. J. A. Baselmans, J. Bueno, S. J. C. Yates, O. Yurduseven, N. Llombart, K. Karatsu, A. M. Baryshev, L. Ferrari, A. Endo, D. J. Thoen, P. J. de Visser, R. M. J. Janssen, V. Murugesan, E. F. C. Driessen, G. Coiffard, J. Martin-Pintado, P. Hargrave, and M. Griffin, A kilo-pixel imaging system for future space based far-infrared observatories using microwave kinetic inductance detectors, *Astron. Astrophys.* **601**, A89 (2017).
- [58] Lorenza Ferrari, Ozan Yurduseven, Nuria Llombart, Stephen J. C. Yates, Juan Bueno, Vignesh Murugesan, David J. Thoen, Akira Endo, Andrey M. Baryshev, and Jochem J. A. Baselmans, Antenna coupled MKID performance verification at 850 GHz for large format astrophysics arrays, *IEEE Trans. Terahertz Sci. Technol.* **8**, 127 (2018).
- [59] CST—Computer Simulation Technology, <https://www.cst.com>.